

**Figure 7.** Simulations for a proton 2.5 Å from the metal center showing the effect of  $g$  anisotropy on ENDOR splitting.  $g_y = 2.05$ ,  $g_z = 2.4$ .

splitting is observed for the peaks created when the field is along the  $g_y$  axis. Even though the field makes a perpendicular angle with the electron-proton vector in each case, the hyperfine energy is different due to anisotropy in the electron  $\bar{g}$  tensor. This effect is observable in experimental ENDOR spectra from randomly oriented samples.

In order to determine nuclear geometries and spin densities from ENDOR spectra, one must be able to determine the correspondence between observed ENDOR peaks and the direction of the molecule in the applied field. The applied field magnitude, along with the EPR parameters, provides information about the field directions that may give rise to ENDOR peaks. Nuclear geometric parameters and field directions used in calculations of ENDOR peak positions with eq 16 must be able to reproduce experimental peak positions for spectra acquired at different field magnitudes. Asymmetry about the free nuclear frequency and dependence of ENDOR shifts on the effective  $g$  value help in the assignment of peaks to specific protons and field orientations. The method is illustrated in the accompanying experimental paper for a polycrystalline copper complex.

### Conclusions

This paper has given the theoretical foundation for a comprehensive analysis of ENDOR powder spectra. We have shown that irradiation of any region of an EPR spectrum allows one to select a distinct group of molecular orientations for acquisition of ENDOR data. Interpretation of ENDOR peaks at one field magnitude must be consistent with interpretations at all other field values, placing stringent conditions on peak assignment and nuclear coordinates. Our derivation of a general equation for ENDOR transition frequencies shows that the equation which has commonly been used to analyze powder ENDOR spectra is incorrect. The correct equation predicts that some powder pattern peaks will occur asymmetrically about the free nuclear frequency and that ENDOR shifts depend on the effective electron  $g$  value.

**Acknowledgment.** This work was supported in part by National Institute of Health Grant GM22793 and by a graduate research fellowship from the Eastman Kodak Co.

## Angle-Selected ENDOR Spectroscopy. 2. Determination of Proton Coordinates from a Polycrystalline Sample of Bis(2,4-pentanedionato)copper(II)

T. A. Henderson, G. C. Hurst, and R. W. Kreilick\*

*Contribution from the Department of Chemistry, University of Rochester, Rochester, New York 14627. Received February 19, 1985*

**Abstract:** Angle-selected ENDOR experiments have been performed with polycrystalline samples of bis(2,4-pentanedionato)palladium(II) doped with Cu(II). These experiments allowed the position and Fermi contact energy for a nearby proton to be determined from a randomly oriented sample. The experiments also confirm theoretical predictions of the asymmetric arrangements of ENDOR peaks with respect to the nuclear Zeeman frequency, the  $g$  value dependence of ENDOR shifts, and the dependence of ENDOR peak intensities on the electron spin quantum number.

Anisotropy in the EPR spectra of noncrystalline metal complexes can be used to select specific molecular orientations with respect to the external magnetic field.<sup>1</sup> The EPR "powder" spectrum arises from randomly oriented molecules but when the field is fixed at a specific value, only molecules at certain orientations contribute to electron resonant absorption. When  $g$  anisotropy dominates the angular dependence of the EPR spectrum, it is convenient to describe the selected molecular orientations with reference to the principal  $\bar{g}$  axis system.<sup>2</sup> Electron nuclear double

resonance (ENDOR) spectroscopy involves setting the external magnetic field to a specific EPR transition and sweeping radio frequency radiation through nuclear transitions while monitoring the EPR absorption. The ENDOR shifts thus obtained reflect electron-nuclear dipolar and Fermi contact hyperfine interactions. If one makes use of the angular selection provided by the EPR field setting, one is able to analyze ENDOR shifts to determine the Fermi contact energy of ligand nuclei and their position with respect to the principal  $\bar{g}$  axis system. Angle-selected ENDOR spectroscopy, therefore, provides a powerful technique for determination of ligand structures in polycrystalline or glassy samples.

The theoretical analysis used in most ENDOR studies of randomly oriented samples has involved some erroneous as-

(1) Hurst, G.; Henderson, T. A.; Kreilick, R. W. *J. Am. Chem. Soc.*, preceding paper in this issue

(2) Abragam A.; Bleaney B. "Electron Paramagnetic Resonance of Transition Metal Ions"; Clarendon Press: Oxford, 1970.

assumptions for calculation of ENDOR transition frequencies and has unnecessarily limited ENDOR observation fields to the turning points of the EPR spectrum. The effect of  $g$  value anisotropy on ENDOR transition frequencies has generally been neglected, resulting in predictions that ENDOR peaks from spin  $1/2$  nuclei should always be symmetrically disposed around the nuclear Larmor frequency. A more complete theory for ENDOR transitions shows that the  $g$  anisotropy must be directly included in the equation for ENDOR shifts and that ENDOR peaks may be asymmetrically disposed about the nuclear Larmor frequency. Asymmetry in ENDOR spectra can be a useful guide to relative nuclear geometries for nuclei which experience a large dipolar field. When ENDOR spectra are recorded at a series of magnetic field values, one is able to select a series of different molecular orientations and completely analyze the hyperfine tensor to determine nuclear positions relative to the  $\bar{g}$  axis system. Experiments of this type can give data from randomly oriented samples that is equivalent to a single-crystal rotation in an external field.

We have taken ENDOR spectra of samples of copper-doped polycrystalline palladium acetylacetonate at a series of EPR field values and analyzed these data to determine proton positions and Fermi contact energies. ENDOR spectra of this molecule show the asymmetric disposition of peaks and the dependence on the effective  $g$  value predicted by the more complete theoretical treatment of ENDOR shifts.<sup>1</sup> With this approach, proton coordinates can be determined from polycrystalline samples with high accuracy.

### Theoretical

Interpretation of ENDOR spectra from randomly oriented samples of transition-metal complexes requires initial analysis of the EPR spectrum to determine the relation between molecular orientations and resonant field values. For a more convenient picture, molecular orientation in the applied field is equated with field direction in the  $\bar{g}$  axis system. In the case of metal complexes, one must often consider the  $\bar{g}$  and metal atom hyperfine anisotropy to determine the field directions that contribute to the EPR spectrum at any given field magnitude. If ENDOR data are collected at a series of EPR field values, the angular dependence of the hyperfine energy can be measured and analyzed to determine the location and contact interaction for ligand nuclei.

The contribution of metal hyperfine and electron  $g$  value anisotropy to the EPR spectrum is well described by the following equations:<sup>2</sup>

$$H_0 = \frac{[h\nu - M_1 A(\theta, \phi)]}{\beta_e g(\theta, \phi)} \quad (1)$$

$$g(\theta, \phi) = \left[ \sum_{i=1}^3 (g_i h_i)^2 \right]^{1/2} \quad (2)$$

$$A(\theta, \phi) = \frac{\left[ \sum_{i=1}^3 \left( \sum_{j=1}^3 A_{ji} g_j h_j \right)^2 \right]^{1/2}}{g(\theta, \phi)} \quad (3)$$

$$h_1 = \cos \phi \sin \theta \quad h_2 = \sin \phi \sin \theta \quad h_3 = \cos \theta$$

$$\vec{H} = [h_1, h_2, h_3] H_0 \quad (4)$$

where  $H_0$  is the resonant field,  $h$  is Planck's constant, and  $\nu$  is the microwave frequency. Angles  $\theta$  and  $\phi$  are field orientation parameters in the  $\bar{g}$  axis system as shown in Figure 1. The solution of eq 1 gives the  $\theta$  and  $\phi$  values which contribute to the resonance at any field value. When the metal  $g$  and hyperfine anisotropy is axial with coincident axes as in  $\text{Cu}(\text{AcAc})_2$ , the  $\phi$  dependence in eq 1-3 vanishes and resonant field values depend only on angle  $\theta$ . The EPR spectrum of  $\text{Cu}(\text{AcAc})_2$  and a diagram which gives the relation between  $\theta$  and  $H_0$  is shown in Figure 2. The paths on the surface of the sphere in Figure 1 represent the field directions that are consistent with the applied fields used in these ENDOR experiments.

ENDOR is performed at field values where particularly simple sets of molecular orientations are selected. Extraction of nuclear

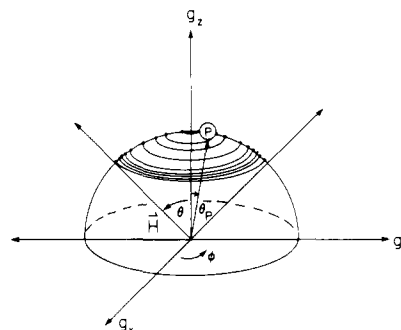


**Figure 1.** Coordinate system in which proton position is defined. Circles indicate the field orientations in the  $g$  axis system that are selected for molecules containing  $^{63}\text{Cu}$  at each of the ten applied fields of the experiment. The dots show which field directions are associated with the observed ENDOR peaks.

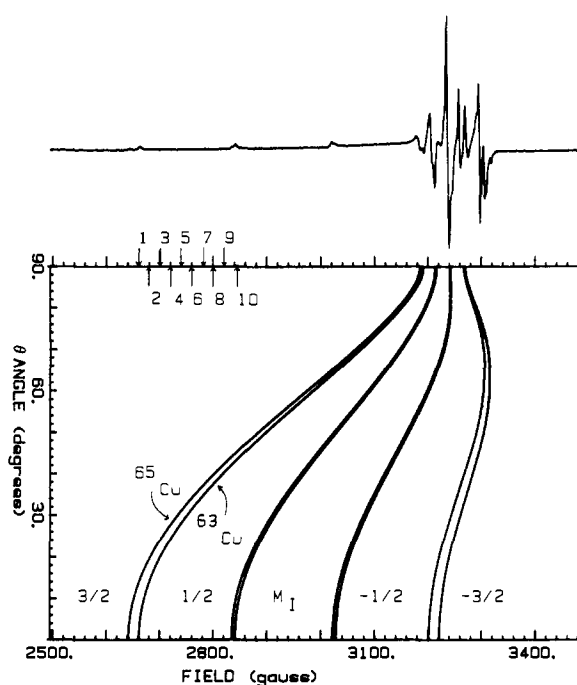


**Figure 2.** Field  $\theta$  given as a function of applied field magnitude, for both isotopes of copper, along with the experimentally measured X-band EPR spectrum.

coordinates from the resulting ENDOR spectra is achieved by associating specific field directions with observed ENDOR peaks. The equations relating ENDOR frequencies to applied field directions are

$$\nu(\vec{H}, m_s) = \left[ \sum_{i=1}^3 \left[ \frac{m_s}{g(\theta, \phi)} \left( \sum_{j=1}^3 g_j h_j A_{ji} \right) - h_i \nu_0 \right]^2 \right]^{1/2} \quad (5)$$

$$\nu_0 = g_N \beta_N H_0 / h$$

$$A_{ij} = \frac{-\beta_e g_N \beta_N}{hr^3} g_i (3r_i r_j - \delta_{ij}) + A_{\text{iso}} \delta_{ij} \quad (6)$$

where  $H_0$  is the applied field magnitude,  $m_s$  is the electron spin quantum number, and  $\nu(\vec{H}, m_s)$  is the nuclear resonant frequency. The elements of the ligand hyperfine tensor,  $A_{ij}$ , are a function of the direction cosines ( $r_i$ ) for the metal-nucleus vector, the metal-nucleus separation  $r$ , the principal  $g$  values, and the isotropic Fermi contact interaction ( $A_{\text{iso}}$ ). Equations 5 and 6 establish the correct correspondence between the observed ENDOR frequencies, the applied field vector, and the nuclear position for complexes having appreciable  $g$  value anisotropy.

For powders of axial complexes, the applied field fixes only the  $\theta$  parameter of field direction. Since the field parameter  $\phi$  can assume a continuous range of values, the ENDOR spectrum shows

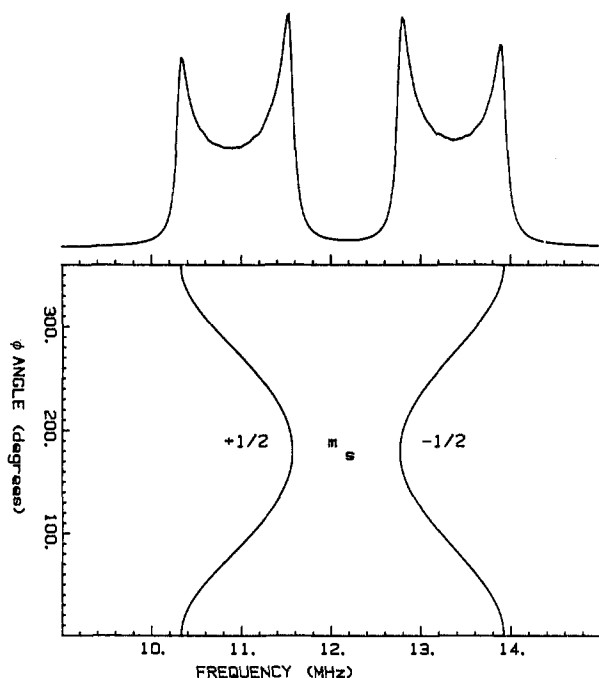


Figure 3. Display of ENDOR frequency as a function of field orientation parameter  $\phi$ . Spectrum at the top indicates the relation between peaks and the  $\phi$  vs. the frequency curve. Parameters used in this example are for proton 1 at an applied field of 2821.44 G (spectrum 9 of Figure 5).

a continuous range of resonant frequencies. Peaks occur in the continuum, however, because the rate of change of ENDOR frequency with  $\phi$  is zero at certain field directions. This fact allows one to assign specific field vectors to observed ENDOR peaks as illustrated in Figure 3. The graph is drawn at constant applied field so that the angle  $\theta$  is constant. Frequencies where the derivative of the curve is infinite correspond to ENDOR peaks associated with specific field angles  $\phi$  and  $\theta$ . Data from ENDOR spectra are thereby reduced to a collection of ENDOR frequencies and associated field vectors which can be used to determine nuclear coordinates.

### Experimental Section

Copper and palladium acetylacetonate were obtained from Aldrich Chemical Co. These complexes were co-crystallized to yield a powder containing about 0.5% copper acetylacetonate. Three millimeter inside diameter quartz samples tubes were used for all experiments. The structure of this copper-doped Pd complex<sup>3</sup> is shown in Figure 4.

**Instrumental.** An IBM/Bruker ER200D EPR spectrometer with a homemade ENDOR cavity and RF sweep unit was used for these experiments. A cylindrical TE011 cavity<sup>4</sup> with internal wires for production of the rf field was employed for both EPR and ENDOR measurements. Nuclear frequencies were generated by a Wavetek Model 3000 which was computer controlled via the sweep unit and frequency modulated with an external source at 19 kHz. An ENI Model 3200L power amplifier was used as the final amplification stage. An Air Products liquid helium transfer system maintained a 100- $\mu$ L sample at a temperature of 5 K. The ENDOR signals were phase sensitive detected with a PAR lock-in amplifier whose output was directed to a home-built Z-80 based computer system for signal averaging.<sup>5</sup> Approximately 100 10-s scans were averaged to achieve an adequate signal-to-noise ratio. The microwave frequency was 9.26 GHz.

### Results

To analyze ENDOR spectra and determine nuclear coordinates, one must measure ENDOR resonant frequencies as the EPR field is set at a series of different values. The low-field region ( $M_1 = +3/2$ ) of a copper EPR spectrum is usually most suitable for

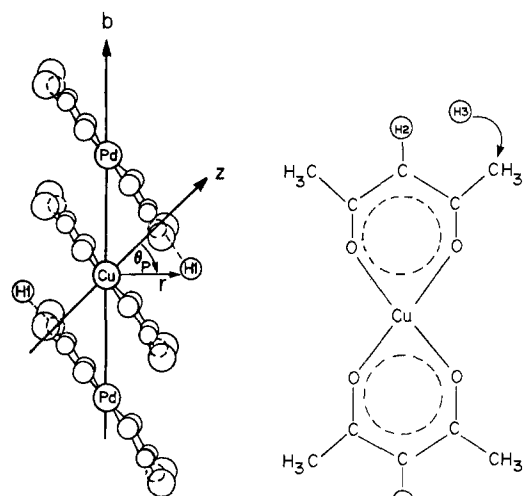


Figure 4. Packing of molecules in the microcrystallite of the powdered sample and the structure of a single  $\text{Cu}(\text{AcAc})_2$  molecule. The coordinates of H1 are determined in this study with high accuracy.

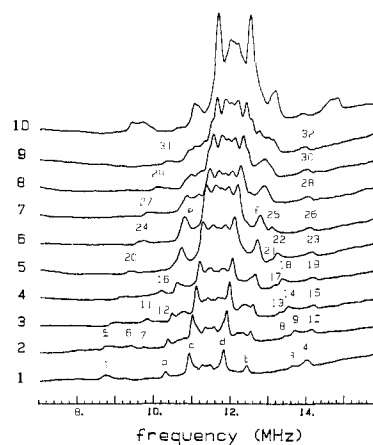


Figure 5. Experimentally obtained ENDOR spectra. Each spectrum was acquired at successive field values as given in Table I. Numbered peaks were used to determine location of proton 1 and lettered peaks refer to resonances of protons 2 and 3.

angular selection as in principle single values of  $\theta$  are selected at these magnetic field settings. The high-field regions of the EPR spectra of copper complexes have contributions from more than one copper spin manifold so that more than one set of orientations is selected at these fields. This region of the spectrum becomes very complicated if a system is not completely axial or if the  $\bar{g}$  and metal hyperfine axes are not fully coincident, so one must exercise caution when using this region of the EPR spectrum for ENDOR experiments.

The EPR and ENDOR spectra given in this paper are complicated by the presence of the two naturally occurring isotopes of copper which have slightly different gyromagnetic ratios and a 2:1 abundance ratio. The number of EPR transitions is doubled because of the different hyperfine coupling to the two copper isotopes. These isotope effects are resolved in some cases (low-field region of Figure 2) or may broaden the EPR line width. The different metal hyperfine energy of the two isotopes also complicates the ENDOR spectra because selected molecular orientation sets are doubled for most fields. Peaks from molecules containing different copper isotopes are clearly resolved in many of the ENDOR spectra.

The ENDOR spectra shown in Figure 5 were taken at the ten EPR field settings indicated in Figure 2. The ENDOR lines with the largest shifts are assigned to the extramolecular methyne proton of a neighboring  $\text{Pd}(\text{AcAc})_2$  molecule (proton 1 of Figure 4) which is closest to the Cu atom in these polycrystalline samples. The ENDOR lines with smaller shifts are assigned to the methyne and methyl protons of the  $\text{Cu}(\text{AcAc})_2$  molecule. The two Cu

(3) Hill, A. E.; Durham, G. S.; Ricci, J. E. *J. Am. Chem. Soc.* **1940**, *62*, 2723.

(4) Hyde, J. S. *J. Chem. Phys.* **1965**, *43*, 1806.

(5) Schultz, R.; Hurst, G.; Thieret, T. E.; Krelick, R. W. *J. Magn. Reson.* **1983**, *53*, 303.

Table I<sup>a</sup>

no.	field, G	$\theta$ , deg	ENDOR frequencies			
			$m_s = +1/2$		$m_s = -1/2$	
			$\phi = 0$	$\phi = 180$	$\phi = 180$	$\phi = 0$
10	2843.89	43.3, 6.4*	9.434*			13.864, 14.787*
9	2821.44	40.4	10.332			13.394
8	2801.45	37.7	10.058			13.996
7	2781.44	34.8	9.804			14.013
6	2761.21	31.7	9.593		13.064	14.057
5	2741.47	28.3 (31.2)	9.320		(13.001) 13.187	14.075
4	2721.52	24.4 (28.0)		10.164	(13.152) 13.328	14.136
3	2701.30	20.0 (24.1)		9.786 (10.041)	(13.275) 13.486	14.136
2	2681.58	14.4 (19.8)	8.714	9.364 (9.698)	(13.407) 13.662	14.101
1	2661.11	3.1 (13.9)	8.696	(9.215)	(13.609)	13.978

<sup>a</sup>Data are presented as it appears in the spectra of Figure 5, i.e., frequency at bottom left corner is no. 1, frequency at top right corner is no. 35. Parentheses indicate that the  $\theta$  value and measured frequency come from a molecule containing <sup>65</sup>Cu. The \* indicates that the data were extracted from the  $M_1 = 1/2$  metal hyperfine manifold.

isotopes present in the sample double the selected field angles, and ENDOR peaks from these different molecules are resolved in some cases (peaks 2, 3, 7, 8, 12, 13, 17, and 21). The frequency of the resolved pairs is consistent with the selected values of  $\theta$  for the two different Cu isotopes. Assignment of peaks to molecules with different Cu isotopes is also confirmed by the 2:1 natural abundance ratio of <sup>63</sup>Cu to <sup>65</sup>Cu which leads to a 2:1 intensity ratio for the ENDOR peaks.

Table I lists the measured ENDOR frequencies for the extramolecular proton (no. 1 of Figure 4). Not all of the 88 possible frequencies are represented because some were obscured by the resonances of protons 2 and 3 or were not sufficiently well-resolved to be measured accurately. Note that frequencies labeled 33 and 35 show the onset of resonance in the  $M_1 = 1/2$  metal hyperfine manifold. These sets of frequencies can be used, along with the values of  $\theta$  associated with the field magnitude at each spectrum, to determine the coordinates and Fermi contact energy for this proton. The proton coordinates obtained are  $\theta_p$ , the angle that the electron-proton vector makes with the  $g_z$  axis,  $r_p$ , the distance of the proton from the copper atom, and  $A_{iso}$ , the Fermi contact term. The  $\phi$  coordinate of the proton is not accessible in axial systems as there is no angular selection in this coordinate. We have used a "least-squares" procedure to find the values for  $r_p$ ,  $\theta_p$ , and  $A_{iso}$  that are most consistent with the sets of frequencies measured at each field value.

The procedure uses eq 5 and 6 and searches the domain defined by  $r_p$ ,  $\theta_p$ , and  $A_{iso}$  to calculate theoretical value for the frequencies represented in Table I. The values in the domain that minimize the squared differences between the experimental and calculated values for all 35 measured frequencies are the coordinates of the proton. The coordinates obtained from the experimental data of Table I are  $r_p = 3.25$  Å,  $\theta_p = 9.7^\circ$ , and  $A_{iso} = 0.28$  MHz. The values are precise to within 0.05 Å, 0.1°, and .05 MHz for  $r_p$ ,  $\theta_p$ , and  $A_{iso}$ , respectively. The average deviation of frequencies from their experimental value was about 20 kHz, with a maximum of 60 kHz. The derived coordinates are in good agreement with the position of the proton deduced from the X-ray crystal structure of the palladium compound<sup>3</sup> which gives  $r_p = 3.01$  Å and  $\theta_p = 19^\circ$ . The discrepancy in the value of  $\theta_p$  between the ENDOR and X-ray determinations may be corrected by the fact that the  $g_z$  axis of the complex is 5.8° removed from an axis completely perpendicular to the plane of the complex.<sup>6</sup> The angle of the proton-copper vector with respect to the new axis is  $\theta_p = 15.5^\circ$ , in much better agreement with the X-ray result. A simulation of the ENDOR spectra for this proton, using eq 5 and 6, is shown in Figure 6.

The data extracted from the powder pattern for this proton are equivalent to that obtained in a single-crystal experiment in which the field is rotated in a plane defined by the  $g_z$  axis and the electron-proton vector. Figure 7 shows the angular dependence of the hyperfine energy for such a rotation, along with the experimentally measured points. This representation is convenient

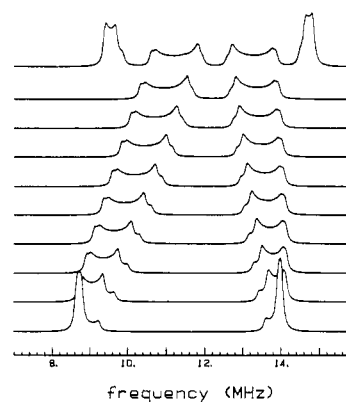


Figure 6. Simulation of spectra for proton 1 including both copper isotopes.

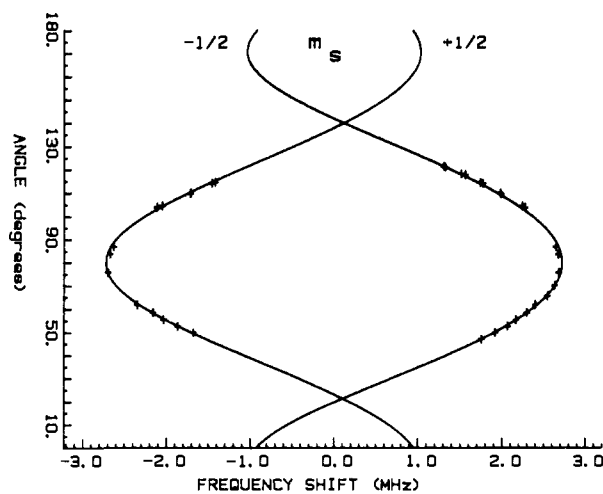


Figure 7. Curves representing the ENDOR shifts that would be obtained for a single-crystal rotation in a plane defined by the  $g_z$  axis and the copper-proton vector. The data of Table I, presented in this form, are indicated as "+" on the curves.

for the data of this particular proton, but in general ENDOR peaks from powders will arise from a diverse collection of field directions.

These results show how it is possible to extract proton positions and contact energies from ENDOR spectra of randomly oriented metal complexes. Equally important is the fact that the characteristics of ENDOR spectra predicted by eq 5 and 6, and discussed extensively elsewhere,<sup>1</sup> are observed experimentally.

The asymmetric arrangement of pairs of ENDOR peaks ( $m_s = \pm 1/2$ ) about the proton Larmor frequency is clearly demonstrated in peaks 31 and 32 of Figure 5. The applied field for this spectrum selects orientations at large displacements from the principal axes of the proton hyperfine tensor and yields the ex-

(6) Kita, S.; Hashimoto, M.; Iwazumi, M. *J. Magn. Reson.* **1982**, *46*, 361.

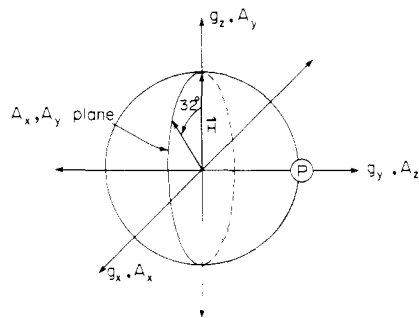


Figure 8. Superposition of  $\bar{g}$  and hyperfine coordinate systems for a proton located in the plane. The change in selected  $\theta$  between spectrum 1 and 6 causes peaks to occur at different directions in the  $A_x, A_y$  plane.

pected shift to higher frequencies for the  $m_s = \pm 1/2$  pair.<sup>7</sup> The average of peaks 31 and 32 is 12.13 MHz, 130 kHz above the proton Larmor frequency. Peaks 5 and 10 are equally placed around the free proton frequency, however, since a selected  $\theta$  of  $10^\circ$  at this field gives peaks corresponding to a field direction very close to the metal-proton vector ( $A_z$  axis).

Information about proton position is also available in the peaks of Figure 5 closer to the Larmor frequency. Selective deuteration studies have shown that peaks a and b and their analogues at higher fields arise from proton 2 of Figure 4 and that peaks c and d in like manner arise from proton 3. It is difficult to analyze peaks in this region with the detail of proton 1, but the intense and well-resolved peaks observed at all fields are characteristic of protons located near the plane of an axial complex. For the relatively low  $g$  anisotropy of this complex, the proton hyperfine tensor is nearly axial. Figure 8 shows an EPR selected orientation superimposed on the hyperfine coordinate system for a planar proton. Since the ENDOR splitting changes very little in the  $A_x, A_y$  plane, the small difference in selected  $\theta$  for the two copper isotopes makes a negligible difference in the ENDOR splitting. This isotope effect explains the sharp line width and strong intensity of pairs a,b and c,d. The pairs of peaks persist at all field values because selection of any  $\theta$  value gives an orientation set that intersects the  $A_x, A_y$  plane.

If the  $g$  anisotropy of the electron was totally ignored, however, one would expect the hyperfine tensor to be completely axial and display a splitting that is independent of selected  $\theta$ . Comparison of pairs e,f with a,b shows the influence of the effective  $g$  value on the symmetry of the hyperfine tensor. The splitting of peaks a,b is 2.11 MHz, while that of peaks e,f at a field  $\theta$   $32^\circ$  larger is 2.0 MHz. Observation of this effect confirms the prediction implicit in eq 5 and 6 that ENDOR shifts depend on effective  $g$  value.

The theoretical treatment of ENDOR spectra from randomly oriented samples<sup>1</sup> predicts that the two branches of the ENDOR

spectrum,  $m_s = +1/2$  and  $m_s = -1/2$ , should have different intensities due to the different frequency shifts in the manifolds. This prediction is confirmed by comparison of the high-end ( $m_s = -1/2$ ) and low end ( $m_s = +1/2$ ) patterns for proton 1 in Figure 5. Resonances within the  $m_s = 1/2$  branch do not span as wide a frequency range as the resonances of the  $m_s = +1/2$  branch; hence, the high-frequency branch appears more intense than the low-frequency branch.

### Discussion

The aim of powder ENDOR spectroscopy is to provide detailed structural information about paramagnetic materials in randomly oriented states. The most interesting samples which might be investigated with this technique are various metal-containing biological molecules as one cannot generally prepare single crystals of these compounds.  $\text{Cu}(\text{AcAc})_2$  was chosen for this investigation to experimentally demonstrate theoretical predictions for ENDOR shifts.<sup>1</sup> This molecule has a relatively simple ENDOR spectrum with well resolved lines and is well suited to test the theoretical predictions. The theory predicts possible asymmetry of shifts with respect to the nuclear Zeeman frequency, an implicit dependence of ENDOR shifts on the effective  $g$  value and a difference in intensities of the two  $m_s$  manifolds in certain circumstances. These predictions are confirmed by the ENDOR spectra of  $\text{Cu}(\text{AcAc})_2$ .

The results of this study with a simple polycrystalline complex also have implication for study of more important molecules. The results have shown that it is helpful to use ENDOR observation fields that give a simple set of selected orientations and to choose these fields so that a continuity in observed peaks exists from one field value to the next. The patterns that emerge from observation at a series of fields provide important clues for determination of nuclear position and Fermi contact energy. Measurement of symmetric and asymmetric pairs and the dependence of ENDOR splitting on the  $g$  anisotropy of the complex further enables one to associate observed peaks with specific field directions and ultimately to analyze the hyperfine interactions in terms of proton coordinates.

### Conclusions

The results obtained for copper-doped palladium acetylacetonate powder demonstrate that accurate values of proton coordinates can be obtained from a polycrystalline sample. Effects such as asymmetry about the free nuclear frequency and effective  $g$  value dependence, previously unreported and unaccounted for in powder ENDOR, are now fully explained and verified. Acquisition of ENDOR spectra at a series of field values, instead of only at the turning points, places stringent conditions on peak assignment and nuclear geometry. Interpretation of the data at one field must be consistent for spectra at all fields. With these more complete methods, assignment of peaks to specific nuclei is facilitated, and accurate nuclear coordinates can be obtained from noncrystalline samples.

**Acknowledgment.** This work was supported in part by National Institute of Health Grant GM22793 and by a graduate research fellowship from the Eastman Kodak Co.

(7) Schweiger, A. "Electron Nuclear Double Resonance of Transition Metal Complexes with Organic Ligands; Structure and Bonding"; Springer-Verlag: New York, 1982; Vol. 51, p 29.